Global analysis of building façade exposure to water penetration in Chile

José M. Pérez-Bella[a], Javier Domínguez-Hernández[a,*], Enrique Cano-Suñén[a], Juan J. del Coz-Díaz[b], Mar Alonso-Martínez[b]

[a] *Department of Construction Engineering, Engineering and Architecture School, University of Zaragoza, María de Luna, s/n, 50018 Zaragoza, Spain.*

[b] *Department of Construction Engineering, University of Oviedo, Edificio Departamental Viesques nº 7, 33204 Gijón, Spain.*

Abstract

In this study, the exposure of building façades in Chile to wind-driven rain and driving rain wind pressure was analysed. Daily climatic data from 29 weather stations throughout Chile were used to determine these exposures in scalar terms and are presented in exposure maps. These values were used to estimate the risk index for water penetration at each location and to determine the relationships between the different exposure indices calculated from the daily, monthly, and annual data. Finally, the directional characterisations of these exposures were determined with an alternative method that was based on climatic data from the Chilean stations. This method was used to quantify the exposure of façades oriented in any direction in 6 cities that represent the country's climate: Santiago, Concepción, La Serena, Temuco, Antofagasta, and Puerto Montt. In general, the exposure of façades to water penetration progressively increases from north to south. However, this pattern is affected by the topography of each location, especially in the capital and southern regions. Valdivia, which is located in the centre, and Balmaceda, which is located in the south, showed the greatest risk of water penetration in Chilean façades.

Keywords

Wind-driven rain; Wind pressure; Water tightness; Risk assessment; Building design; Chile

* Corresponding author. Department of Construction Engineering, University of Zaragoza, María de Luna, s/n, 50018, Zaragoza, Spain. Tel.Fax: +34 976 76 21 00.
E-mail address: javdom@unizar.es (Javier Domínguez-Hernández)

1. Introduction

Wind during atmospheric precipitation adds a horizontal component to the velocity of each raindrop, which may affect vertical surfaces such as building façades [1]. This phenomenon (wind-driven rain or WDR) is the primary cause of liquid water build-up on building enclosures. Moreover, when combined with the concurrent wind pressure that is exerted on the façade (driving rain wind pressure or DRWP), increases the risk of humidity penetration into the building [2-4].

In addition, the penetration of atmospheric water into façade materials alters the habitability of the building and affects occupant health [5, 6]. This penetration reduces the thermal insulation provided by these materials [7, 8] and has a number of adverse effects (e.g., corrosion, chemical attack, frost damage, salt transport, efflorescence, discoloration, soiling, loss of adherence, biological growth, deformation, cracking, etc.) that increase the maintenance costs for the building [9-14].

To design building enclosures that prevent or limit the penetration of atmospheric water, the exposure of façades to driving rain and simultaneous wind pressure must be characterised at each location [15]. Thus, multiple researchers have attempted to determine the WDR and DRWP in different locations and countries [16-23]. However, only a few researchers have conducted directional studies for both exposures to determine the exposures of all façade orientations at multiples locations.

The objective of this study was to determine the WDR and DRWP in scalar terms for various locations in Chile subjected to different climates, from the northern desert regions (e.g., Atacama desert) to the southern subantarctic zones (e.g., the archipelago of Tierra del Fuego). The overall exposure of these façades to water penetration was characterised by combining both scalar exposures into a single integrated index (Risk Index of Water Penetration or RIWP) [24].

This scalar characterisation was complemented by a directional distribution analysis of both exposures relative to various building façade orientations. A new calculation method that uses climatic data, which are normally recorded by weather stations in Chile, is suggested in this study. This method was applied to 6 cities distributed throughout Chile that represent the country's diverse climatic conditions.

Overall, this study establishes a complete characterisation method (both scalar and directional) for the climatic exposures that are most relevant for water penetration in building façades in Chile. This characterisation can be used with the indicators and maps presented to improve building design by establishing normative requirements adjusted for the exposure characteristics of each location.

2. Background

Atmospheric water that hits the facades due to WDR and the concurrent DRWP are the main causes of unwanted humidity penetration into buildings [25]. Thus, all tests used to determine the maximum water tightness of a façade system must recreate extreme conditions that represent both exposure parameters [26-28].

Regarding the primary cause of humidity penetration into façades without significant pores or fissures (<1 mm), various studies have indicated that the presence of water is less important than the concurrent wind pressure [3]. Therefore, water tightness tests that are usually applied to new and relatively flawless enclosures use pressure difference as the main test parameter. However, in deteriorated façades (i.e., those with defects or fissures >5 mm), the presence of water becomes the main parameter because it can penetrate the enclosure even in the absence of significant wind pressure [29].

Due to the variety of materials, finishes and conservation or maintenance states of the façades, neither of these parameters can be ignored when characterising the global risk of water penetration. Thus, determining the WDR and DRWP façade exposure conditions in each location is a required preliminary step for optimising their design.

Several researchers have used semi-empirical methods to characterise WDR exposure, which enabled them to obtain approximate results from the recorded climatic data at each location [30, 31]. The general formulation of these methods (called the "WDR relationship") allows for assessing the WDR_θ (mm) that hits a façade of orientation θ (º) by using wind direction D (º), wind velocity U (m/s) and rain R_h (mm) records from each location (Eq. 1). This relationship is fit by using an empirical coefficient k that varies with precipitation type and is usually between 0.2 and 0.25 s/m [32, 33].

$$WDR_\theta = k \cdot U \cdot R_h \cdot \cos\left(D - \theta\right) \tag{1}$$

This relationship was recently standardised in ISO 15927-3:2009 [34], setting the coefficient k to $2/9$ s/m and using an exponential fit (see Eq. 2). In addition, hourly wind and precipitation data, which were simultaneously recorded over N years, were used (a historic series of more than 10 years was preferred) as a reference for calculating the yearly average wind-driven rain $WDR_{A\theta}$ (mm). Moreover, the wind velocity U_{10} (m/s) must be recorded under standardised conditions at a height of 10 m on clear terrain without obstacles [35].

$$WDR_{A\theta} = \frac{2}{9} \cdot \frac{\sum_{i=1}^{m} U_{10i} \cdot \left(R_{hi}\right)^{8/9} \cdot \cos\left(D_i - \theta\right)}{N} \tag{2}$$

To quantify the amount of water hitting a façade orientation θ, only the m intervals during which the wind direction D drives the precipitation over the façade's surface must be considered in the summation (see Fig. 1) [36].

Fig. 1. Cosine projection method for the semi-empirical calculation of wind-driven rain over a particular façade with an orientation θ [36].

However, this standard is rarely used because many countries do not have hourly climatic data for multiple locations that were collected over a period of more than 10 years. Moreover, the absence of simultaneous wind direction records usually prevents the generalisation of these directional calculations and restricts them to specific stations [37]. Thus, in recent years, various studies have attempted to obtain directional results that are comparable to those of the ISO standard, which is based on more frequently collected climatic data (e.g., synoptic data recorded 6 or 8 times a day) [38, 39].

All of these limitations have forced studies that are aimed at characterising exposure over vast areas to use formulations based on the available climatic data from more weather stations. Thus, the annual Driving Rain Index (aDRI) is the most commonly WDR exposure measure in many countries [1, 19-23].

This index, which is a simplification of the WDR relationship, ignores the empirical fitting coefficient k and determines the annual exposure $aDRI$ (m^2/s) as the product of m precipitation records R_h (mm) and wind velocities U_{10} (m/s) obtained over a period of N years at each location (see Eq. 3). Generally, the directional component is disregarded. Consequently, the obtained characterisation is scalar and does not account for the differences between the specific exposures of every possible enclosure orientation [40].

$$aDRI = \frac{\sum_{i=1}^{m} U_{10i} \cdot \left(\frac{R_{hi}}{1000} \right)}{N} \tag{3}$$

The annual average rain and wind velocity (*aaDRI*), the monthly average (*maDRI*), or the daily average (*daDRI*) data can be used to calculate this index. Because the average-related error and the error of the simultaneity between the wind and rain recordings are lower, the greater the data recording frequency is, the more precise are the indices [41, 42].

Due to their simplicity, these indices are efficient tools for comparing the WDR exposure of different locations with limited climatic data. Although this index does not quantify the WDR that affects the

façades, some studies have been conducted to establish empirical fitting coefficients that relate the obtained *aDRI* values (m^2/s) to the quantity of WDR that is received by the building enclosure [43].

Moreover, Bernoulli's equation can be used to characterise the exposure of a façade with an orientation θ (º) to wind pressure $DRWP_\theta$ (Pa) concurrent with WDR [3], where U (m/s) and D (º) represent the velocity and direction records, respectively, for the winds that occur with significant precipitation (>0.05 mm). For this calculation, a pressure coefficient C_p of 1 and an air density ρ_{air} of 1.2 kg/m^3 (Eq. 4) can be used in the absence of more accurate data.

$$DRWP_\theta = C_p \cdot \frac{1}{2} \cdot \rho_{air} \cdot U^2 \cdot \cos\left(D - \theta\right) \tag{4}$$

To determine the average DRWP exposure, the average of the m $DRWP_\theta$ exposures over the number of years being considered can be used (Eq. 5). Only records where the wind direction D creates a positive wind pressure over the surface of the enclosure should be considered in the summation (see Fig. 1). Furthermore, the wind velocity value U_{10} (m/s) should be obtained by using the same standardised recording conditions that are established for Equations 2 and 3 (a height of 10 m on a clear terrain with no obstacles).

$$DRWP_{A\theta} = \frac{\sum_{i=1}^{m} \frac{1}{2} \cdot \rho_{air\ i} \cdot {U_{10i}}^2 \cdot \cos\left(D_i - \theta\right)}{m} \tag{5}$$

As for *aDRI*, the use of more frequent wind records results in more accurate DRWP exposure estimates by precisely identifying the direction D associated with the velocity data U_{10} and by dismissing wind records that do not occur with significant precipitation.

Similar to WDR exposure, the wind pressure during WDR can be characterised by scalar terms when wind direction data are unavailable. In this case, the directional component must be eliminated from the

general expression, and all *m* records that occur simultaneously with rain must be considered in the summation (Eq. 6).

$$DRWP_A = \frac{\sum_{i=1}^{m} \frac{1}{2} \cdot \rho_{air\ i} \cdot U_{10i}{}^2}{m} \quad (6)$$

The previous equations (Eq. 3 and 6) may be used to evaluate the risk of water penetration on the enclosures by characterising the two climatic parameters that are most relevant to such penetration in the same location (i.e., WDR and DRWP). The scalar or directional nature of this characterisation and its accuracy will only depend on the quality of the available climatic records from the various weather stations selected for the analysis.

In Section 3.2 of this work, the exposures of 29 Chilean cities are analysed in scalar terms using daily climatic data for each location collected over 10 years. This scalar analysis is completed in Section 3.3 by calculating the RIWP [24] and by establishing a single, qualitative classification for the water penetration risk on the façades in the different studied locations. In addition, the relationships between the scalar indices (*aaDRI*, *maDRI*, and *daDRI*) are examined and compared to those of other countries.

Section 4 concludes by suggesting a new alternative method of characterisation for the directional distribution of the WDR and DRWP exposures. For this purpose, the proposed method only uses daily precipitation data and wind frequency and intensity reports for a limited number of directions. This method has been used to determine both directional exposures for 6 major Chilean cities.

3. The scalar characterisation of WDR and DRWP in Chile

3.1 The Chilean perspective

Analysing previous exposures in Chile is interesting because geographic and atmospheric conditions vary widely throughout this territory. The large coast running along the country (from a latitude of 18ºS to 55ºS, excluding the Antarctic territory) covers over 4,000 km and encompasses diverse climatic regions with different patterns of humidity exposure on the façades.

The Andes cause significant changes in altitude in the eastern part of the country and reach heights of up to 6,000 meters in some locations that are less than 200 km from the coast (Ojos del Salado volcano). This mountain range also isolates the country from the humid air masses of the continent (rain shadow phenomenon) and increases the influence of the South-Eastern Pacific subtropical anticyclone, Humboldt Current, and Hadley cell on the country's climate (Fig. 2).

This subtropical anticyclone is perennially located between 30ºS and 80ºW and induces stable, high-pressures conditions that prevent precipitation fronts in the northern region of Chile [44]. However, air currents generated by the anticyclone from the south transport oceanic humidity and can generate mist in this region. The Humboldt Current accentuates the lack of precipitation on the North Coast by dragging cold water to the oceanic surface, which reduces superficial evaporation and convective cloud formation [45]. These effects are enhanced by the Hadley cell, which transports dry air from the atmospheric layers [46]. Consequently, the northern part of the country (latitudes 18ºS to 30ºS) has a very arid climate with precipitation of less than 1 mm/year (e.g., Arica, Iquique and Atacama desert airports).

Low-pressure systems can move to the southern coast, which is far from these influences, and cause predominately west-east winds that transport oceanic humidity and favour precipitation. Thus, the southern climate of the country is rainy with prolonged wet seasons (the precipitation rates are greater than 1,500 mm/year south of a latitude of 42ºS and it is impossible to define a dry summer). In addition, the low temperatures from the advanced latitudes further south progressively increase snow precipitation.

The centre of the country has a transitional climate that is conditioned by topographic height, with progressively more abundant precipitation from north to south. Consequently, several main climate subtypes exist in Chile, including desert, Mediterranean, continental, and oceanic climates [47].

Fig. 2. Locations of the weather stations used in this study and the most relevant geographic/atmospheric factors that impact the Chilean climate.

3.2 WDR and DRWP analysis

Since 1884, the Meteorological Directorate of Chile (DMC) has been charged with providing meteorological services to the country. Currently, the DMC possesses historic climate data collected from various locations [48]. In this study, 29 weather stations located in the continental part of the country and the Juan Fernández Islands were selected (Table 1). Most of these stations are located in airports and aerodromes near urban centres. Thus, their climatic conditions can be considered similar to those of neighbouring cities.

Table 1. Summary of the analysed Chilean weather stations.

All of the stations have climatic data records for precipitation and wind. These data were collected for at least 10 years (November 2002 - October 2012). The precipitation data corresponded to 4 daily recordings (at 6-hour intervals), from which the total daily rainfall can be calculated. Regarding wind velocity and direction, daily reports of frequency and intensity are available based on a variable number of recordings

(8 to 24 daily observations, depending on the station). These reports contain the number of daily observations where the wind direction can be associated with one of the 8 main geographic orientations (frequency *F*). In addition, these reports contain the average velocity associated with each direction (intensity *I*) (see Table 2). The "Variable" direction (Vrb) encompasses records in which a specific wind direction cannot be assigned. In contrast, the "Calm" designation encompasses records in which the wind velocity was negligible.

Table 2. Example of ten daily reports for wind velocity and direction (*data: Jan. 2011, Santiago-Quinta Normal*).

With these meteorological records, the WDR and DRWP exposures for the various locations analysed could be characterised in scalar terms by using Equations 3 and 6. Thus, the *daDRI* (m^2/s), *maDRI* (m^2/s), and *aaDRI* (m^2/s) indices were used to determine the scalar exposure to WDR for each location based on the average daily, monthly and annual precipitation R_h (mm) and wind velocity U_{10} (m/s) data, respectively (see Eq. 3).

The daily precipitation for each location can be obtained by adding the 4 daily observations for each station. From the total daily values, the total monthly or yearly values can be calculated for the N =10 year historical series.

To obtain the daily average wind velocity values from the frequency and intensity reports that were available from the Chilean stations, the intensity records for each of the D=8 main geographic orientations were averaged for each day i (Eq. 7). In addition, "Variable" direction measurements were also incorporated to accurately estimate the average value.

$$U_{10i} = \frac{F_{Vrb\,i} \cdot I_{Vrb\,i} + \sum_{D=1}^{8} F_{D\,i} \cdot I_{D\,i}}{Total\ records_i} \quad (7)$$

The monthly and annual wind velocity averages were calculated from the daily averages for each location. These averages were used to determine the *maDRI* and *aaDRI* indices. Fig. 3 geographically represents the WDR exposure characterisation based on the *daDRI* value. This index is presented with the *maDRI* and *aaDRI* values in Table 3.

Fig. 3. WDR exposure map of Chile.

A constant air density value ρ_{air} of 1.2 kg/m^3 was used in the scalar $DRWP_A$ (Pa) calculation (see Eq. 6) and the average wind velocities were obtained from Eq. 7. Only the *m* average wind velocity values, which correspond to days with significant precipitation (>0.05 mm), were considered for this calculation. The $DRWP_A$ values obtained by following this method are shown in Fig. 4 and are detailed in Table 3.

Fig. 4. DRWP exposure map of Chile.

Table 3. Scalar characterisation of WDR and DRWP exposure for 29 Chilean cities *(data: November 2002- October 2012).*

3.3 Risk Index of Water Penetration

Once the WDR and DRWP exposure values were calculated, they can be combined to create a single index that includes the severity of both parameters that are most relevant for the water penetration process. This risk index of water penetration (or *RIWP*) can be used to compare the combined exposure from various locations by characterising the overall water penetration risk [24]. For this purpose, each exposure parameter associated with a location *j* is normalised with respect to the maximum and minimum values identified from the available sample base (Eq. 8 and 9).

$$daDRI_{normalised\ j} = \frac{daDRI_j - daDRI_{\min}}{daDRI_{\max} - daDRI_{\min}} \tag{8}$$

$$DRWP_{A\ normalised\ j} = \frac{DRWP_{A\,j} - DRWP_{A\min}}{DRWP_{A\max} - DRWP_{A\min}} \tag{9}$$

Both normalised values (oscillating between 0 and 1) were combined in Eq. 10 to obtain the *RIWP* for each location. Thus, greater normalised values correspond to increased risk of water penetration at the location. Both exposures were assumed to influence the penetration process equally. Therefore, the obtained index can be used for façades with different surface finishes, where the influence of one exposure may oscillate relative to the influence of another [3].

$$RIWP_j = \sqrt{\left(daDRI_{normalised\ j}\right)^2 + \left(DRWP_{A\ normalised\ j}\right)^2} \tag{10}$$

The results for the 29 considered locations are presented in Table 3. This calculation identified the locations with similar risks of water penetration and established quantitative limits that can be used to determine the best-adapted façade design for each risk level. Based on previously suggested limits [24], Fig. 5 indicates the Chilean locations with moderate ($0.4 \leq RIWP < 0.7$), high ($0.7 \leq RIWP < 1.0$), or severe ($RIWP \geq 1.0$) risks.

Fig. 5. Classification of locations with greater risk of water penetration in Chile. *Only sites with radii (i.e. RIWP values) that are at risk of water penetration greater than 0.4 were named.*

3.4 Scalar results and discussion

As expected, the WDR exposure in the considered locations significantly varied from negligible in the north (Iquique, 0.0002 m^2/s) to greater than 8 m^2/s in Valdivia (centre of the country). However, these values are within the characteristic range of other countries, such as Greece, Nigeria, Spain, and Turkey [20-23], and below the characteristic range of humid countries, such as India or Ireland [19, 49].

In general, the *daDRI* value progressively increased from the north to Puerto Montt and decreased again further south. The conditions at Santiago (with indices of less than 0.6 m^2/s) must be highlighted because this area is highly protected by calm winds that dominate the area during the winter months (when the majority of precipitation occurs). Further south, Chile Chico can also be considered as a protected location. Here, the rain shadow caused by the nearby mountains that separate this location from the Pacific Ocean, significantly reduces its average annual precipitation and exposure to WDR.

When comparing the WDR exposure indices calculated from either average daily or monthly data, fitting can be used to estimate the *daDRI* value from the monthly average wind velocity and precipitation (Fig. 6). A similar fit can be determined to estimate the *daDRI* value from annual average data (Fig. 7). Both expressions can be useful when accurately estimating the WDR exposure in Chilean locations where the availability of weather data is limited.

Fig. 6. Best fit-linear relationship between *daDRI* and *maDRI*.

Fig. 7. Best fit-linear relationship between *daDRI* and *aaDRI*.

The existing relationship between the *maDRI* and *aaDRI* was analysed for the 29 locations (Fig. 8). This relationship is similar to those observed in other countries (e.g., Greece, Nigeria, and Spain), which suggested that it could be extrapolated to other regions. In addition, this situation differs from the situation in other countries where greater precipitation rates and seasonal atmospheric phenomena (e.g., India) may cause significant error.

Fig. 8. Best fit-linear relationship between *maDRI* and *aaDRI,* and a comparison between different countries.

Moreover, the DRWP exposure values fluctuate from 0.57 Pa in Santiago to 34.67 Pa in Balmaceda. There is no clear distribution pattern that characterises these exposures because high $DRWP_A$ values can be observed in the north (Calama, 26.81 Pa) and South (Balmaceda; Punta Arenas, 29.61 Pa; Puerto Williams, 23.38 Pa; Chile Chico, 17.93 Pa). The lowest DRWP exposure values in Chile were found in and near Santiago due to the calm winds that characterise the rainy season.

To characterise this exposure using climatic records collected in any location of Chile, Fig. 9 depicts the relationship between the average wind pressure and the previously calculated $DRWP_A$ values at each location. The average wind pressure was calculated by using an air density of 1.2 kg/m^3 and the average wind velocity for each day of the studied period, regardless of precipitation. This mathematical fit includes an acceptable coefficient of determination R^2 and indicates how the wind pressure during rainfall

in the considered locations is generally less in Chile than the average wind pressure (represented by the dots below the broken line in Fig. 9).

Fig. 9. Best fit-linear relationship between $DRWP_A$ and *mean wind pressure*.

Furthermore, the *RIWP* indicates that 55% of the analysed locations (16 out of 29) can be regarded as a low risk for water penetration (*RIWP*<0.4). However, more than 80% of locations are regarded as low risk in other countries, such as Spain [24]. In addition, the high risk value identified in Valdivia is mainly due to the large volume of WDR received by the façades. However, the similar risk value for Balmaceda is due to the high wind pressure that coincided with precipitation.

Thus, two groups of locations are distinguishable in Figure 5. First, Balmaceda, Punta Arenas, Puerto Williams and Chile Chico have significant risk levels due to their high wind pressure, which facilitates water penetration into buildings despite the small volume of WDR. Calama is peculiar due to its low annual precipitation and WDR (5.7 mm/year; *daDRI* 0.023 m^2/s), which makes the penetration of enclosures by water unlikely (despite the high DRWP exposure). In contrast, Valdivia, Puerto Montt, Osorno, Chillán and Temuco have a significantly greater risk of water penetration mainly due to the WDR rather than the concurrent wind pressure.

As expected, the risk of water penetration in Santiago is abnormally low considering its annual precipitation rate and geographic position in the centre of the country (Santiago, 0.03; Tobalaba, 0.05; Pudahuel, 0.11). The trajectory of precipitation in this city, which is normally vertical due to the absence of simultaneous wind, protects the vertical enclosures from atmospheric rain. This protection results in negligible water penetration risk on the façades.

The above scalar results provide a useful estimate of the mean exposure conditions in the country using the climatic data available. However, the driving rain indices calculated do not provide the quantity of WDR (l/m^2) and the exposure values should be adjusted for façades without standardised conditions (at a height of 10 m on clear terrain without obstacles).

Moreover, the time interval of exposure is also an important factor to be considered. Usually, the water penetration into building façades does not develop throughout a complete year but intensifies during short time intervals [34]. Thus, the peak values of wind velocity and precipitation associated with wetting stages could be more important than mean values and should also be considered for a future comprehensive characterisation of the exposure in the country.

4. Directional characterisation of WDR and DRWP in Chile

The simultaneous occurrence of WDR and DRWP over the various façades of a building can vary greatly in its orientation and normal rain and wind conditions. Thus, it is important to quantify the directional distribution of exposure to optimise façade designs for different locations.

The precipitation records and wind frequency and intensity reports that are available from the Chilean stations do not include hourly data and cannot be directly used in the directional calculations of ISO 15927-3:2009 (see Eq. 2). However, these data can be used to estimate the directional distribution of both exposures with a new calculation process, which is explained below. This method was used to estimate the directional distribution of WDR and DRWP exposures in 6 major Chilean cities throughout the country (Antofagasta, La Serena, Santiago, Concepción, Temuco and Puerto Montt).

Before performing a directional characterisation of the WDR exposure in the studied locations, the total daily precipitation R_h (mm) must be proportionally distributed among the directions analysed by the

weather stations, including the "variable" and "calm" directions (Eq. 11). For this purpose, the daily wind frequency distribution F_D for each direction and the total records for each day i were used (see Table 2).

$$R_{hi\,D} = R_{hi} \cdot \frac{F_{D\,\mathrm{i}}}{Total\ records_i} \tag{11}$$

Once known, the daily precipitation distribution $R_{h\,D}$ (mm) and the average daily wind intensity I_D (m/s) for each direction can be used to determine the directional component $daDRI_D$ (m^2/s) for each of the main D=8 orientations (Eq. 12). This equation considers the m daily precipitation records collected throughout the considered N years (November 2002-October 2012).

$$daDRI_D = \frac{\sum_{i=1}^{m}\left[I_{D\,\mathrm{i}} \cdot \left(\frac{R_{hi\,D}}{1000}\right) + I_{Vrb\,\mathrm{i}} \cdot \left(\frac{R_{hi\,Vrb}}{1000}\right) \cdot \left(\frac{F_{D\,\mathrm{i}}}{Total\ records_i - F_{Vrb\,\mathrm{i}} - F_{calm\,\mathrm{i}}} \right) \right]}{N} \tag{12}$$

It is assumed that rain in the "calm" direction does not increase WDR on the façades. Moreover, the contribution of WDR from the "variable" direction was proportionally distributed among the 8 main orientations based on the number of records F_D associated with each direction. The number of records with "variable" direction can be used for this calculation and oscillated from 0.9% in Santiago to 23% in Temuco for the 6 locations discussed in this section.

Fig. 10 shows the component $daDRI_D$ that is associated with each of the main geographic orientations for the 6 analysed cities. As expected, the sum of the 8 directional components yields the previously calculated scalar *daDRI* value for each location.

Fig. 10. Directional component of the *daDRI* value for the 8 main geographical directions (m^2/s) in six major cities in Chile.

The directional decomposition of the scalar *daDRI* into its main orientations can be used to estimate the average annual WDR for any possible enclosure orientation. For this estimation, Eq. 13 was based on the same cosine projection method used in ISO 15927-3:2009 (see Figure 1). The only elements required for this calculation are the directional components $daDRI_D$, which are associated with a direction D (º) that increases the WDR over a façade at orientation θ (i.e., between $\theta \pm 90º$). For example, to calculate the index of exposure over a façade with a 60º north orientation ($daDRI_{60º}$), the summation must include the following components: $daDRI_N$, $daDRI_{NE}$, $daDRI_E$, and $daDRI_{SE}$.

$$daDRI_\theta = \sum daDRI_D \cdot \cos\left(D - \theta\right) \tag{13}$$

Fig. 11 shows the calculated directional characterisation of the WDR exposures for each of the previously considered cities for façades with orientations of θ at 15º intervals. In addition, this calculation can be extrapolated to any weather station with wind frequency and intensity reports for a limited number of directions.

Fig. 11. Directional *daDRI* values (m^2/s) for 6 major cities in Chile (a*ngles are measured in degrees from the north*).

A similar process was followed to use data recorded by Chilean weather stations to estimate the directional distribution of the DRWP exposure. Thus, the average daily wind velocity $U_{10\,\theta}$ (m/s) perpendicular to a specified orientation θ (º) was estimated from the intensity I_D (m/s) and frequency F_D records gathered during the day from the analysed directions, including the "variable" direction (Eq. 14).

Both summations only need to consider records in which the direction D may induce a positive wind pressure on the orientation under analysis (i.e., those within the interval $\theta \pm 90º$). Again, wind records

associated with the "variable" direction were proportionally distributed among the 8 main geographic orientations because it was impossible to assign them to a specific direction.

$$U_{10i\ \theta} = \frac{\sum\left(F_{D\ \mathrm{i}} \cdot I_{D\ \mathrm{i}} + F_{Vrb\ \mathrm{i}} \cdot I_{Vrb\ \mathrm{i}} \cdot \frac{F_{D\ \mathrm{i}}}{Total\ records_i - F_{Vrb\ \mathrm{i}} - F_{calm\ \mathrm{i}}} \right) \cdot \cos\left(D - \theta\right)}{\sum\left(F_{D\ \mathrm{i}} + F_{Vrb\ \mathrm{i}} \cdot \frac{F_{D\ \mathrm{i}}}{Total\ records_i - F_{Vrb\ \mathrm{i}} - F_{calm\ \mathrm{i}}} \right)} \tag{14}$$

Once the average wind velocity perpendicular to an orientation θ is known for each day i, the average exposure $DRWP_{A\,\theta}$ (Pa) can be calculated from Eq. 15 by using a constant air density ρ_{air} of 1.2 kg/m^3 and by considereing all m daily velocities $U_{10\,\theta}$ occurred on days with significant precipitation (>0.05 mm). Fig. 12 shows the results for façade orientations with 15º intervals in the 6 cities.

$$DRWP_{A\ \theta} = \frac{1}{2} \cdot \rho_{air} \cdot \frac{\sum_{i=1}^{m} \left(U_{10i\ \theta}\right)^2}{m} \tag{15}$$

Fig. 12. Directional $DRWP_A$ values (Pa) for 6 major cities in Chile (a*ngles are measured in degrees from the north*).

4.1 Directional results and discussion

Figs. 11 and 12 indicate that both exposures have a similar directional distribution in the studied locations. The main WDR exposures in Antofagasta and Santiago are oriented to the south. The greatest values in Concepción, Temuco, and Puerto Montt were obtained for orientations that were approximately northward. In La Serena, the greatest WDR exposure occurred for the east and west orientations.

Similarly, the maximum DRWP value for Antofagasta was for southern orientations, while the maximum DRWP values for Concepcion, Temuco and Puerto Montt were for north-northeast orientations. However, in La Serena, the greatest WDR exposure was achieved along the western orientation. In this city, the most intense precipitation occurs simultaneously with eastern winds, which increase the *daDRI* in this direction. In contrast, the strongest winds that occurred simultaneously with rain came from the west.

An analogous situation occurred in Santiago, where the WDR exposure was much greater for the façades with a southern orientation, despite the similar DRWP exposures of the northern and southern orientations (Table 4). The north-south orientations of the main exposures in the capital were consistent with the topographic conditions of its surrounding terrain. The city is flanked by two mountain ranges to the east and west, which protect it from east and west winds.

This method provides a new alternative for estimating mean directional exposures in countries where the available climatic data are incompatible with ISO 15927-3:2009. In this case, only daily precipitation records and wind frequency-intensity reports for a limited number of directions are needed. However, as for the scalar analysis, peak values of wind velocity and precipitation associated with wetting stages should also be considered for a complete characterisation of the directional exposure. Moreover, the proposed method can lead to some uncertainty in locations with a large number of "variable" direction records, due to the proportional distribution applied in Eqs. 12 and 14.

Table 4. Comparison of the scalar indices and maximum directional values for the WDR and DRWP exposures.

Finally, the scalar exposure values that were initially obtained for each location were related to the maximum directional value identified for a façade orientation. As shown in Fig. 13, the maximum directional exposure for the 6 locations can be estimated by using the scalar exposure results.

Fig. 13. Best fit-linear relationships between the scalar and maximum directional values for the WDR and DRWP exposures.

The high coefficients of determination for both fits suggest that these expressions could be used to estimate the maximum directional exposure in the analysed Chilean locations with only limited climatic data or in the absence of wind direction data. These relationships could be used to assign homogeneous designs for all building façades by using the maximum predicted directional value for the location.

5. Conclusions

This study presents a global analysis of building exposure to WDR and DRWP in Chile. Scalar WDR and DRWP exposure values were determined for various locations throughout the country and characterised under different climatic conditions. These results were used to identify several mathematical relationships for estimating exposure values based on available climatic records from all weather stations. In addition, combining both exposures into a risk index of water penetration has been used to assess the overall risk for each location. Furthermore, various exposure and risk maps have been created to improve the design of Chilean façades by adapting them to the operating conditions that are predicted for each location.

Design optimisation also requires identifying the directional distribution of the WDR and DRWP exposures. Thus, a new calculation process is required that uses climatic data from Chilean weather

stations. This method was used to estimate the directional exposure in 6 major Chilean cities. In addition, the suggested calculation process is potentially an alternative for countries and regions where available climatic data do not comply with the ISO 15927-3:2009 requirements. The directional results suggest that it is possible to estimate the maximum directional exposure with only the characteristic scalar exposure for each location. This method could be useful for assigning a homogeneous design for all façades based on the maximum estimated directional value, even in locations of Chile with no directional weather records.

Acknowledgments

These results were obtained from data provided by the Meteorological Directorate of Chile, General Directorate of Civil Aviation (DCM). This work was partial financed by the Spanish Ministry of Science and Innovation co-financed with FEDER funds under the Research Project BIA2012-31609. We also recognise Javier Jiménez Sevillano for his help in the data collection and processing.

References

[1] Blocken B, Carmeliet, J. A review of wind-driven rain research in building science. J. Wind Eng Ind Aerodyn 2004; 92(13):1079-130. doi:10.1016/j.jweia.2004.06.003.

[2] Blocken B, Derome J, Carmeliet J. Rainwater runoff from building facades: A review. Building and Environment 2013; 60:339-61. doi:10.1016/j.buildenv.2012.10.008.

[3] Cornick SM, Lacasse MA. A review of climate loads relevant to assessing the watertightness performance of walls, windows, and wall-window interfaces. J ASTM Int 2005; 2(10):1-16. doi: 10.1520/JAI12505.

[4] Pérez JM, Domínguez J, Rodríguez B, del Coz JJ, Cano E. A new method for determining the water tightness of building façades. Building Research & Information 2013; 41(4):401-14. doi:10.1080/09613218.2013.774936.

[5] Bornehag CG, Blomquist G, Gyntelberg F, Järvholm B, ; Malmberg P, Nordvall L, et al. Dampness in building and health. Indoor Air 2001; 11:72-86. doi:10.1034/j.1600-0668-2001-110202.x.

[6] WHO. Environmental burden of disease associated with inadequate housing. Methods for quantifying health impacts of selected housing risks in the WHO European region. Copenhagen: World Health Organization; 2011.

[7] Sanders C. Heat, air and moisture transfer in insulated envelope parts: Environmental conditions. International Energy Agency, Annex 24, Final report, vol. 2. Leuven: 1996.

[8] Del Coz JJ, Rabanal FP, García PJ, Domínguez J, Rodríguez B, Pérez JM. Hygrothermal properties of lightweight concrete: Experiments and numerical fitting study. Construction and Building Materials 2013; 40:543-55. doi: 10.1016/j.conbuildmat.2012.11.045.

[9] Boyd DW. Weather and the deterioration of buildings materials. In: ASTM Special Technical Publication no. 691. Durability of Building Materials and Components. Ottawa: DBR-P-933; 1980, p. 145-56.

[10] Camuffo D, del Monte M, Sabbioni C, Vittori O. Wetting, deterioration and visual features of stone surfaces in an urban area. Atmos Environ 1982; 16(9):2253-9. doi:10.1016/0004-6981(82)90296-7.

[11] Rousseau J. Rain penetration and moisture damage in residential construction. In: Building science insight'83, seminar on humidity, condensation and ventilation in houses. Canada: 1983.

[12] Lipfert FW. Atmospheric damage to calcareous stones: comparison and reconciliation of recent experimental findings. Atmos Environ 1989;23(2):415-29. doi:10.1016/0004-6981(89)90587-8.

[13] Franke L, Schumann I, van Hees R, van der Klugt L, Naldini S, Binda L, et al. Damage atlas: classification and analyses of damage patterns found in brick masonry. European Commission Research report nr 8, vol 2. Fraunhofer IRB Verlag; 1998.

[14] Tang W, Davidson CI, Finger S, Vance K. Erosion of limestone building surfaces caused by wind-driven rain. 1. Field measurements. Atmospheric Environment 2004; 38(33): 5589-99. doi:10.1016/j.atmosenv.2004.06.030.

[15] Kvande T, Lisø KR. Climate adapted design of masonry structures. Building and Environment 2009; 44(12):2442-50. doi:10.1016/j.buildenv.2009.04.007.

[16] Boyd, DW. Driving rain map of Canada. Technical note no. 398. Ottawa: National Research Council Canada; 1963.

[17] Lacy RE. An Index of Exposure to Driving Rain. Garston: Building Research Establishment; 1971. Building Research Station, Digest No. 127.

[18] Welsh RE, Skinner WR, Morris RJ. A climatology of driving rain pressure for Canada. Climate and Atmospheric Research Directorate Draft Report, Environment Canada, Atmospheric Environment Service; 1989.

[19] Chand I, Bhargava PK. Estimation of driving rain index for India. Building Environ 2002; 37: 549-54. doi:10.1016/S0360-1323(01)00057-9.

[20] Akingbade FOA. Estimation of driving rain index for Nigeria. Architectural Science Review 2004; 47(2):103-106. doi:10.1080/00038628.2004.9697032.

[21] Sahal N. Proposed approach for defining climate regions for Turkey based on annual driving rain index and heating degree-days for building envelope design. Building Environ 2006; 41: 520-6. doi:10.1016/j.buildenv.2005.07.004.

[22] Giarma C, Aravantinos D. Estimation of building components' exposure to moisture in Greece based on wind, rainfall and other climatic data. J Wind Eng Ind Aerodyn 2011; 99: 91-102. doi:10.1016/j.jweia.2010.12.001.

[23] Pérez JM, Domínguez J, Rodríguez B, del Coz JJ, Cano E. Estimation of the exposure to moisture in Spain from daily wind and rain data. Building Environ 2012; 57: 259-70. doi:10.1016/j.buildenv.2012.05.010.

[24] Pérez JM, Domínguez J, Rodríguez B, del Coz JJ, Cano E. Combined use of wind-driven rain and wind pressure to define water penetration risk into building façades: the Spanish case. Building Environ 2013;64:46-56. doi:10.1016/j.buildenv.2013.03.004.

[25] Sahal N, Lacasse MA. Experimental assessment of water penetration and entry into siding-clad wall specimen (Internal Report 862). Institute for Research in Construction, National Research Council Canada, Ottawa: 2004.

[26] EN 12865:2001 Hygrothermal performance of building components and building elements. Determination of the resistance of external wall systems to driving rain under pulsating air pressure, European Committee for Standardization.

[27] AS/NZA 4284:2008 Testing of building Façades. Australian and New Zealand Standards Institution.

[28] ASTM E331-00:2009 Standard test method for water penetration of exterior windows, skylights, doors, and curtain walls by uniform static air pressure difference. American Society for Testing and Materials.

[29] Lacasse MA, O'Connor T, Nunes SC, Beaulieu P. Report from Task 6 of MEWS Project: Experimental assessment of water penetration and entry into wood-frame wall specimens – Final Report. (Internal Report 113). Institute for Research in Construction, National Research Council Canada, Ottawa: 2003.

[30] Hoppestad S. Slagregn i Norge (*Driving rain in Norway, in Norwegian*). Norwegian Building Research Institute Report no. 13, Oslo: NBI; 1955.

[31] Lacy RE. Driving-rain maps and the onslaught of rain on buildings. Proceedings of RILEM/CIB symposium on moisture problems in buildings, Helsinki: 1965.

[32] Lacy RE. Climate and Building in Britain. Her Majesty's Stationery Office, London: 1977.

[33] Straube JF, Burnett EFP. Simplified Prediction of Driving Rain Deposition. In: Proc. of International Building Physics Conference, p. 375-382, Eindhoven: 2000.

[34] EN ISO 15927-3:2009 Hygrothermal performance of buildings — Calculation and presentation of climatic data Part 3: Calculation of a driving rain index for vertical surfaces from hourly wind and rain data. European Committee for Standardization.

[35] WMO. Guide to Meteorological Instruments and Methods of Observation. WMO-No 8. World Meteorological Organization, Geneva: 2008.

[36] Blocken B, Carmeliet J. On the validity of the cosine projection in wind-driven-rain calculations on buildings. Building Environ 2006; 41(9): 1182-1189.doi:10.1016/j.buildenv.2005.05.002.

[37] Fazio P, Mallidi SR, Zhu D. A quantitative study for the measurement of driving rain exposure in the Montreal region. Building Environ 1995; 30(1):1-11. doi: 10.1016/0360-1323(94)E0028-P.

[38] Rydock J. Validation of a present weather observation method for driving rain mapping. Building Environ 2007; 42:566-571. doi:10.1016/j.buildenv.2005.09.017.

[39] Pérez JM, Domínguez J, Rodríguez B, del Coz JJ, Suñén E. Optimised method for estimating directional driving rain from synoptic observation data. J Wind Eng Ind Aerod 2013; 113: 1-11. doi: 10.1016/j.weia.2012.12.001.

[40] Prior MJ. Directional driving rain indices for the United kingdom – computation and mapping. Building Research Stablishment, Garston: 1985.

[41] Blocken B, Carmeliet J. On the error associated with the use of hourly data in wind-driven rain calculations on building facades. Atmos Env 2007; 41(11): 2335-43. doi:10.1016/j.atmosenv.2006.11.014.

[42] Blocken B, Carmeliet J. Guidelines for the required time resolution of meteorological input data for wind-driven rain calculations on buildings. J Wind Eng Ind Aerodyn 2008; 96(5): 621–39. doi:10.1016/j.jweia.2008.02.008.

[43] Henriques FMA. Quantification of wind-driven rain. An experimental approach. A general review on driven rain and details of an experiment in Portugal to supplement existing research results in Norway, the UK and elsewhere. Building Research & Information 1992; 20 (5): 295-97. doi: 10.1080/09613219208727227.

[44] Sinclair MR. A climatology of anticyclones and blocking for the southern hemisphere. Monthly Weather Review 1996; 124(2): 245–63. doi: 10.1175/1520-0493(1996)124<0245:ACOAAB>2.0.CO;2.

[45] Khodayar S, Kalthoff N, Fiebeig-Wittmaack M, Kohler M. Evolution of the atmospheric boundary-layer structure of an arid Andes Valley. Meteorol Atmos Phys 2008; 99:181-98. doi: 10.1007/s00703-007-0274-3.

[46] Johanson CM, Fu Q. Hadley cell widening: Model simulations versus observations. Journal of Climate 2009; 22(10): 2713–25. doi: 10.1175/2008JCLI2620.1.

[47] Kottek M, Grieser J, Beck C, Rudolf B, Rubel F. World map of the Köppen-Geiger climate classification updated. Meteorol. Z. 2006; 15:259-63. doi: 10.1127/0941-2948/2006/0130.

[48] Meteorological Directorate of Chile, General Directorate of Civil Aviation. Current and Historical Climatological Products. http://164.77.222.61/climatologia/ (Accessed 15 July 2013)

[49] Walsh S. Distribution of driving rain in Ireland. Irish Meteorological Service, Climatological Note No. 13, Dublin: 2010.

List of tables

Table 1.
Summary of the analysed Chilean weather stations.

WEATHER STATION	ALT. (m)	LATITUDE (DD)	LONGITUDE (DD)	Mean rainfall (mm)
Arica airport	63	-18.3514º	-70.3358º	0.5
Iquique airport	52	-20.5467º	-70.1772º	0.6
Calama aerodrome	2293	-22.4953º	-69.9044º	5.7
Antofagasta (*Cerro Moreno airport*)	113	-23.4503º	-70.4411º	1.7
Atacama desert airport	204	-27.2639º	-70.7742º	0.1
La Serena (*La Florida aerodrome*)	142	-29.9172º	-71.2003º	78.5
Valparaiso aerodrome	330	-33.0367º	-71.5342º	372.5
Santo Domíngo aerodrome	75	-33.6550º	-71.6142º	325.0
Santiago (*Quinta Normal*)	527	-33.4450º	-70.6828º	312.5
Tobalaba aerodrome	650	-33.4544º	-70.5478º	347.2
Pudahuel Santiago	480	-33.5419º	-70.7944º	261.6
Juan Fernández	35	-33.6367º	-78.8350º	1041.5
Curico aerodrome	225	-34.9664º	-71.2167º	701.9
Chillán aerodrome	151	-36.5872º	-72.0400º	1107.0
Concepción (*Carriel Sur airport*)	12	-36.7792º	-73.0622º	110.1
Los Ángeles aerodrome	120	-37.4028º	-72.4200º	1074.4
Temuco (*Maqueue aerodrome*)	92	-38.7700º	-72.6369º	1157.4
Valdivia aerodrome	18	-39.6511º	-73.0817º	1871.0
Osorno aerodorme	61	-40.6050º	-73.0608º	1331.8
Puerto Montt (*El Tepual aiport*)	85	-41.4350º	-73.0975º	1802.5
Futaleufu aerodrome	350	-43.1892º	-71.8492º	2081.0
Alto Palena aerodrome	281	-43.6117º	-71.8053º	1622.3
Puerto Aysén aerodrome	11	-45.3961º	-72.6639º	2313.1
Coyhaique aerodrome	310	-45.5939º	-72.1086º	1205.9
Balmaceda aerodrome	520	-45.9125º	-71.6933º	611.6
Chile Chico aerodrome	328	-46.9086º	-71.6931º	305.5
Lord Cochrane aerodrome	196	-47.2444º	-72.5861º	738.2
Punta Arenas airport	39	-53.0050º	-70.8439º	375.7
Puerto Williams aerodrome	30	-54.9317º	-67.6156º	467.3

Table 2.
Example of ten daily reports for wind velocity and direction (*data: Jan. 2011, Santiago-Quinta Normal*).

Day *i*	Frequency $F^{(1)}$ and Intensity $I^{(2)}$ distribution																		Total records
	N		NE		E		SE		S		SW		W		NW		VRB		Calm		
	F	**I**	**F**	**I**	**F**	**I**	**F**	**I**	**F**	**I**	**F**	**I**	**F**	**I**	**F**	**I**	**F**	**I**	**F**	**I**	
01	-	-	-	-	-	-	-	-	-	-	*4*	*4*	*1*	*7*	-	-	-	-	*3*	*0*	8
02	-	-	-	-	-	-	-	-	*3*	*3*	*4*	*5*	-	-	-	-	-	-	*1*	*0*	8
03	-	-	-	-	-	-	-	-	*1*	*5*	*4*	*4*	*2*	*2*	-	-	-	-	*1*	*0*	8
04	-	-	-	-	-	-	*1*	*2*	*5*	*5*	*1*	*5*	*1*	*2*	-	-	-	-	-	-	8
05	-	-	-	-	-	-	-	-	*1*	*1*	*3*	*4*	*2*	*1*	-	-	-	-	*2*	*0*	8
06	-	-	-	-	-	-	-	-	-	-	*5*	*4*	-	-	-	-	-	-	*3*	*0*	8
07	-	-	-	-	-	-	-	-	*5*	*3*	*3*	*7*	-	-	-	-	-	-	-	-	8
08	-	-	-	-	-	-	-	-	*4*	*3*	*2*	*5*	-	-	-	-	-	-	*2*	*0*	8
09	-	-	-	-	-	-	-	-	*3*	*3*	*2*	*7*	-	-	-	-	-	-	*3*	*0*	8
10	-	-	-	-	-	-	-	-	*4*	*4*	*4*	*3*	-	-	-	-	-	-	-	-	8

$F^{(1)}$: Number of records; $I^{(2)}$: Average wind velocity (knots).

Table 3.
Scalar characterisation of WDR and DRWP exposure for 29 Chilean cities *(data: November 2002- October 2012)*.

WEATHER STATION	*daDRI* (m^2/s)	*maDRI* (m^2/s)	*aaDRI* (m^2/s)	$DRWP_A$ (Pa)	*RIWP* (-)
Arica airport	0.0014	0.0016	0.0018	3.2075	0.08
Iquique airport	0.0002	0.0003	0.0003	6.0734	0.16
Calama aerodrome	0.0230	0.0275	0.0285	26.8083	0.77
Antofagasta (*Cerro Moreno airport*)	0.0067	0.0067	0.0069	6.2123	0.17
Atacama desert airport	0.0420	0.0350	0.0363	9.7356	0.27
La Serena (*La Florida aerodrome*)	0.1825	0.1677	0.1860	2.9696	0.07
Valparaiso aerodrome	2.2488	1.4838	1.6986	8.6166	0.36
Santo Domíngo aerodrome	1.2393	0.9890	1.2023	4.3292	0.19
Santiago (*Quinta Normal*)	0.2184	0.1893	0.2973	0.5740	0.03
Tobalaba aerodrome	0.3645	0.2910	0.4055	0.9384	0.05
Pudahuel Santiago	0.5045	0.3917	0.5222	3.6724	0.11
Juan Fernández	3.4945	3.3655	3.5096	14.5449	0.59
Curico aerodrome	1.9576	1.3544	1.5394	0.8910	0.24
Chillán aerodrome	3.9686	2.5771	2.4561	3.6718	0.49
Concepción (*Carriel Sur airport*)	5.1037	3.2755	3.2457	11.4504	0.70
Los Ángeles aerodrome	4.0993	3.0139	3.2552	11.4127	0.59
Temuco (*Maqueue aerodrome*)	3.2119	2.3983	2.3505	4.3155	0.41
Valdivia aerodrome	8.2073	5.3865	5.3001	10.6756	1.04
Osorno aerodorme	4.3794	3.4571	3.5173	7.8475	0.57
Puerto Montt (*El Tepual aiport*)	6.2741	4.5984	4.3988	7.6171	0.79
Futaleufu aerodrome	2.9399	3.4576	3.6516	5.6772	0.39
Alto Palena aerodrome	2.1613	2.7994	2.9798	5.2674	0.30
Puerto Aysén aerodrome	1.9285	2.2245	1.8511	4.5294	0.26
Coyhaique aerodrome	2.9476	2.6946	2.8220	5.3725	0.39
Balmaceda aerodrome	3.3785	3.4897	3.8041	34.6703	1.08
Chile Chico aerodrome	0.6578	0.8789	1.0583	17.9298	0.52
Lord Cochrane aerodrome	1.1098	1.3775	1.4653	5.1490	0.19
Punta Arenas airport	2.5018	2.5277	2.5505	29.6148	0.90
Puerto Williams aerodrome	1.6242	1.4436	1.3568	23.3785	0.70

Table 4.
Comparison of the scalar indices and maximum directional values for the WDR and DRWP exposures.

WEATHER STATION	*daDRI* (m^2/s)	*max. daDRI*$_\theta$ (m^2/s)		*DRWP*$_A$ (Pa)	*max. DRWP*$_{A\,\theta}$ (Pa)	
Antofagasta	0.0067	0.0041	(180º)	6.2123	6.3231	(180º)
La Serena	0.1825	0.0850	(105º)	2.9696	3.4532	(270º)
Santiago	0.2184	0.1275	(195º)	0.5740	1.1680	(180º)
Concepción	5.1037	4.3290	(0º)	11.4504	13.7345	(0º)
Temuco	3.2119	2.0893	(15º)	4.3155	4.0049	(270º)
Puerto Montt	6.2741	5.3088	(0º)	7.6171	9.4865	(0º)

Figure captions

Fig. 1. Cosine projection method for the semi-empirical calculation of wind-driven rain over a particular façade with an orientation θ [36].

Fig. 2. Location of the weather stations used in this study and the most relevant geographic/atmospheric factors that impact the Chilean climate.

Fig. 3. WDR exposure map of Chile.

Fig. 4. DRWP exposure map of Chile.

Fig. 5. Classification of locations with greater risk of water penetration in Chile. *Only sites with radii (i.e. RIWP values) that are at risk of water penetration greater than 0.4 were named.*

Fig. 6. Best fit-linear relationship between *daDRI* and *maDRI*.

Fig. 7. Best fit-linear relationship between *daDRI* and *aaDRI*.

Fig. 8. Best fit-linear relationship between *maDRI* and *aaDRI*, and a comparison between different countries.

Fig. 9. Best fit-linear relationship between $DRWP_A$ and *mean wind pressure*.

Fig. 10. Directional component of the *daDRI* value for the 8 main geographical directions (m^2/s) in six major cities in Chile.

Fig. 11. Directional *daDRI* values (m^2/s) for 6 major cities in Chile (*angles are measured in degrees from the north*).

Fig. 12. Directional $DRWP_A$ values (Pa) for 6 major cities in Chile (*angles are measured in degrees from the north*).

Fig. 13. Best fit-linear relationships between scalar and maximum directional values for the WDR and DRWP exposures.

Figure 1

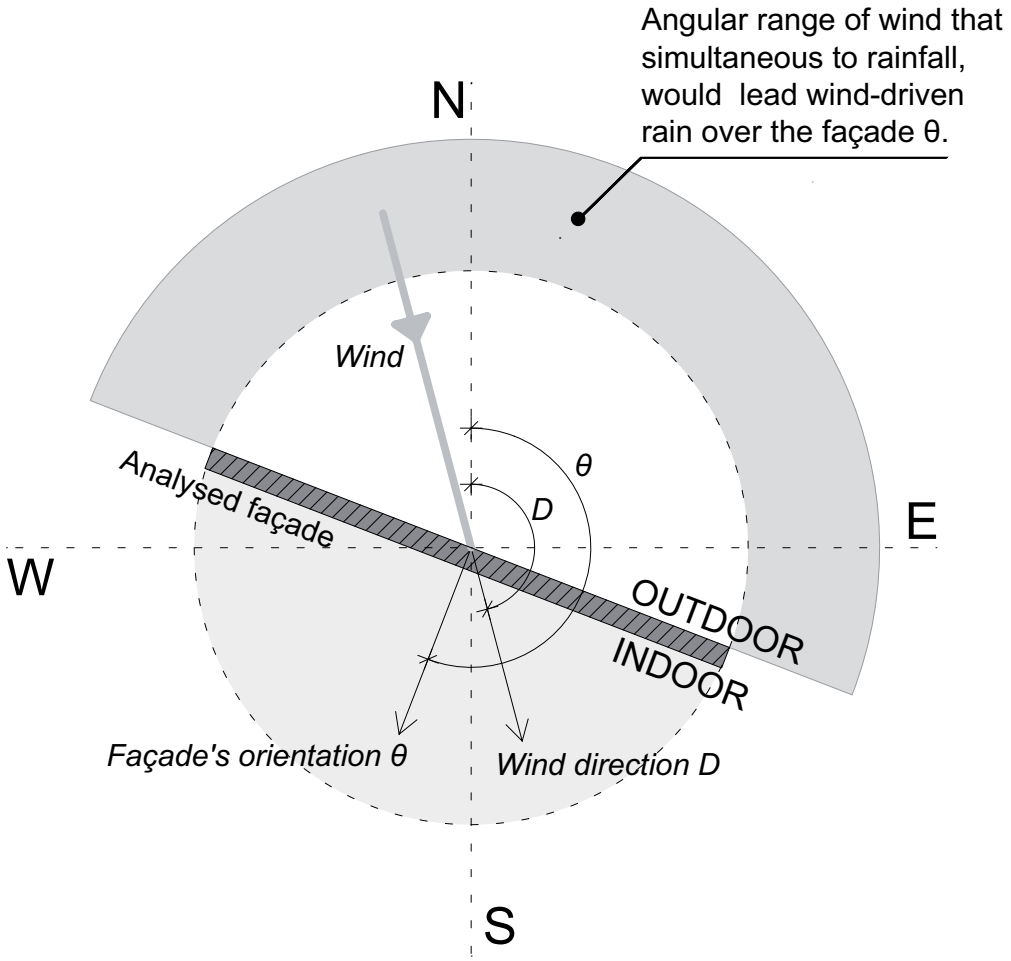

Fig. 1. Cosine projection method for the semi-empirical calculation of wind-driven rain over a particular façade with an orientation θ [36].

Figure 2

Fig. 2. Location of the weather stations used in this study and the most relevant geographic/atmospheric factors that impact the Chilean climate.

Figure 3

Fig. 3. WDR exposure map of Chile.

Figure 4

Fig. 4. DRWP exposure map of Chile.

Figure 5

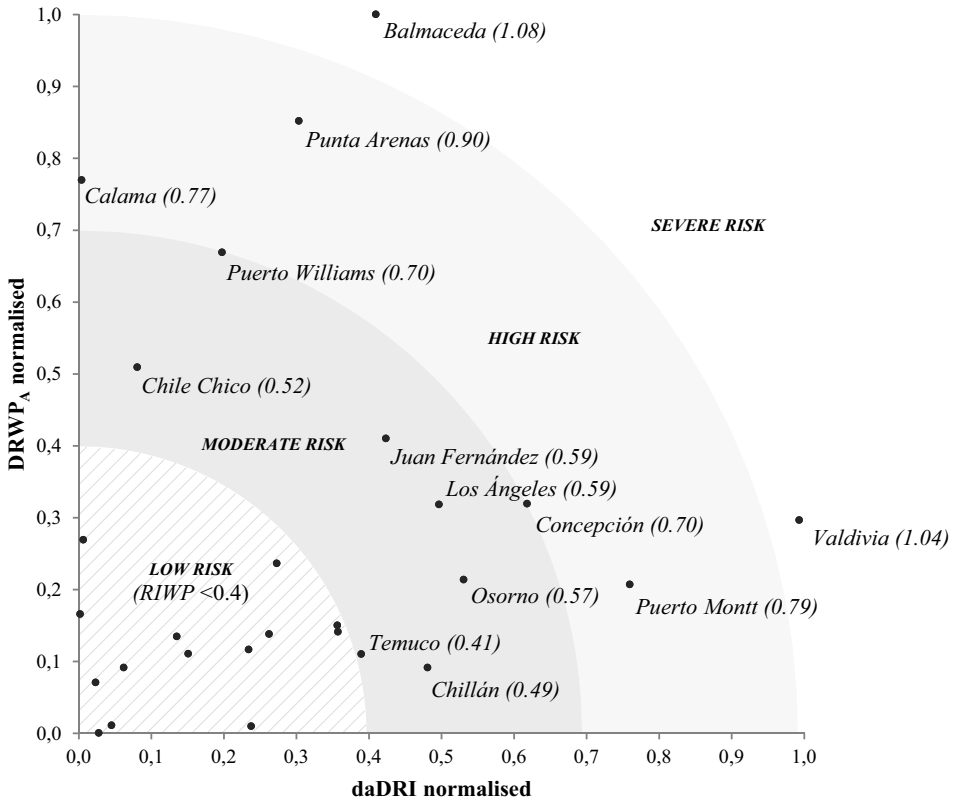

Fig. 5. Classification of the locations with greater risk of water penetration in Chile. *Only sites with radii (i.e. RIWP values) that are at risk of water penetration greater than 0.4 are named.*

Figure 6

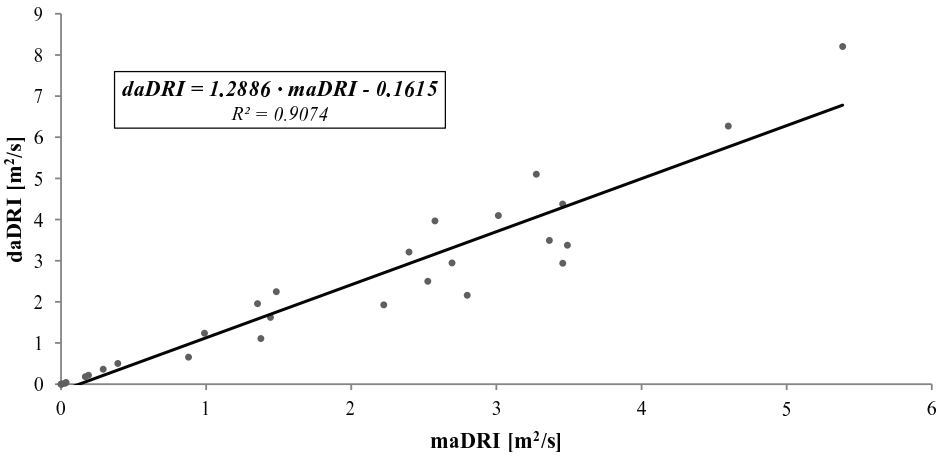

Fig. 6. Best fit-linear relationship between *daDRI* and *maDRI*.

Figure 7

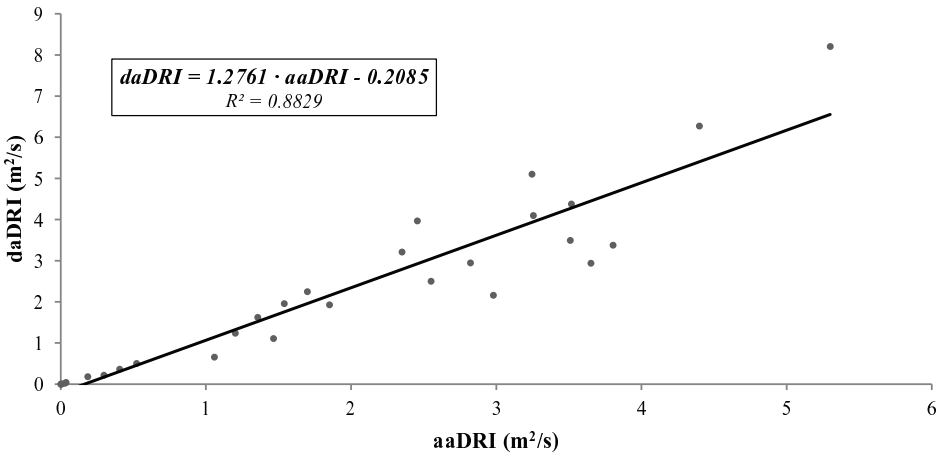

Fig. 7. Best fit-linear relationship between *daDRI* and *aaDRI*.

Figure 8

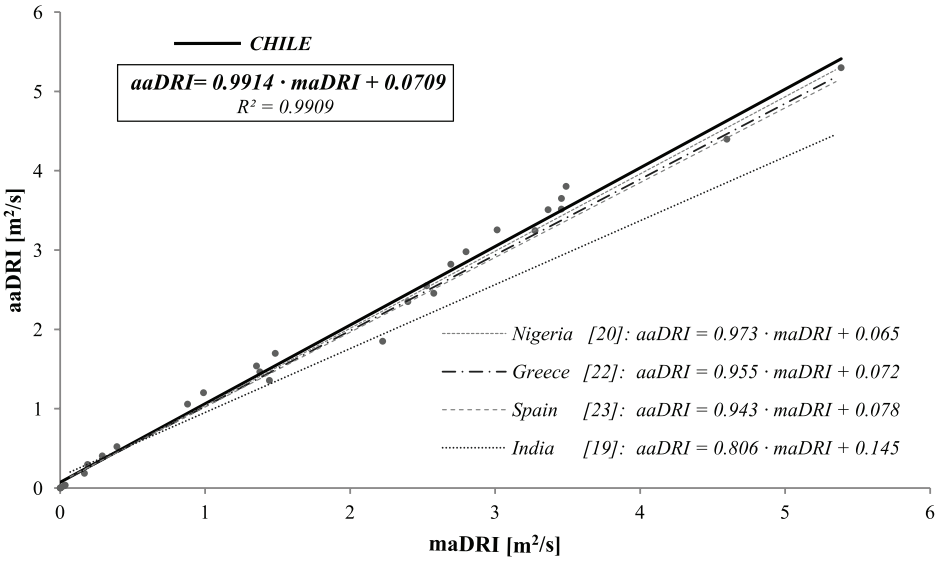

Fig. 8. Best fit-linear relationship between *maDRI* and *aaDRI*, and a comparison between different countries.

Figure 9

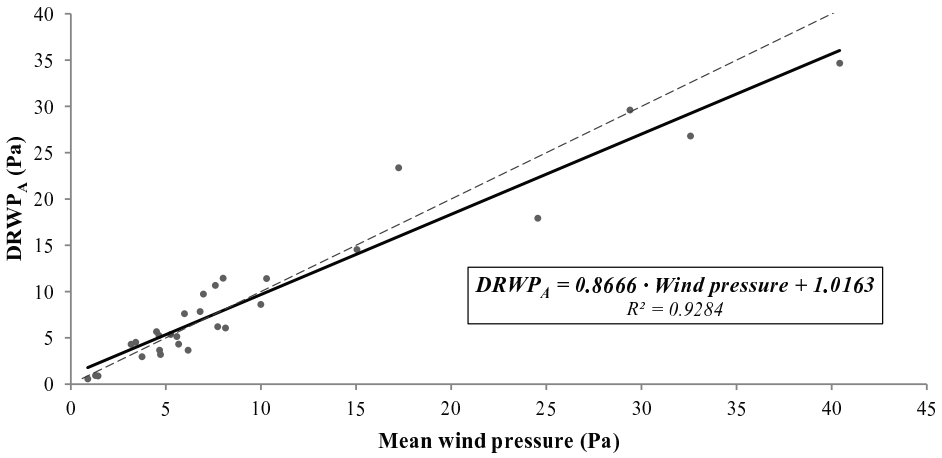

Fig. 9. Best fit-linear relationship between $DRWP_A$ and *mean wind pressure.*

Figure 10

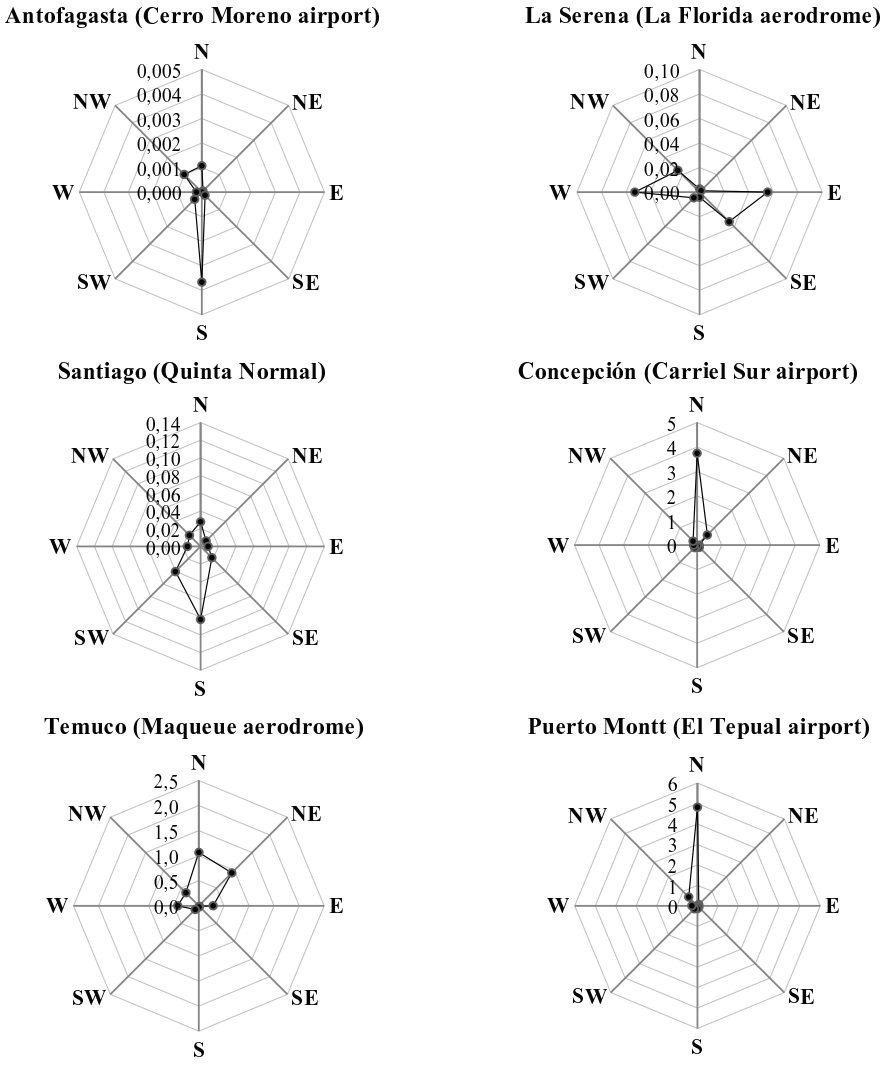

Fig. 10. Directional component of the *daDRI* value for the 8 main geographical directions (m^2/s) in six major cities in Chile.

Figure 11

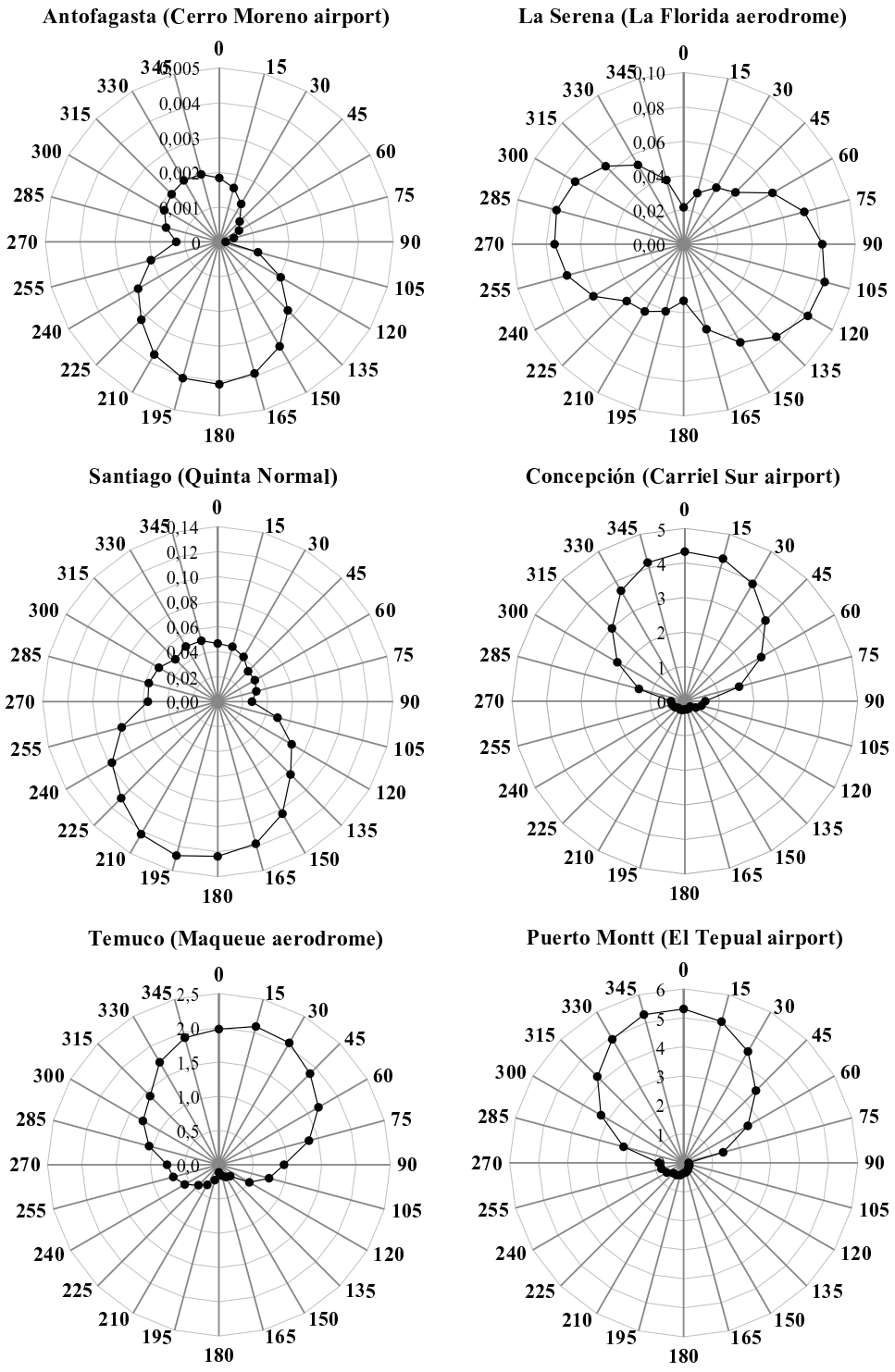

Fig. 11. Directional *daDRI* values (m^2/s) for 6 major cities in Chile (a*ngles are measured in degrees from north*).

Figure 12

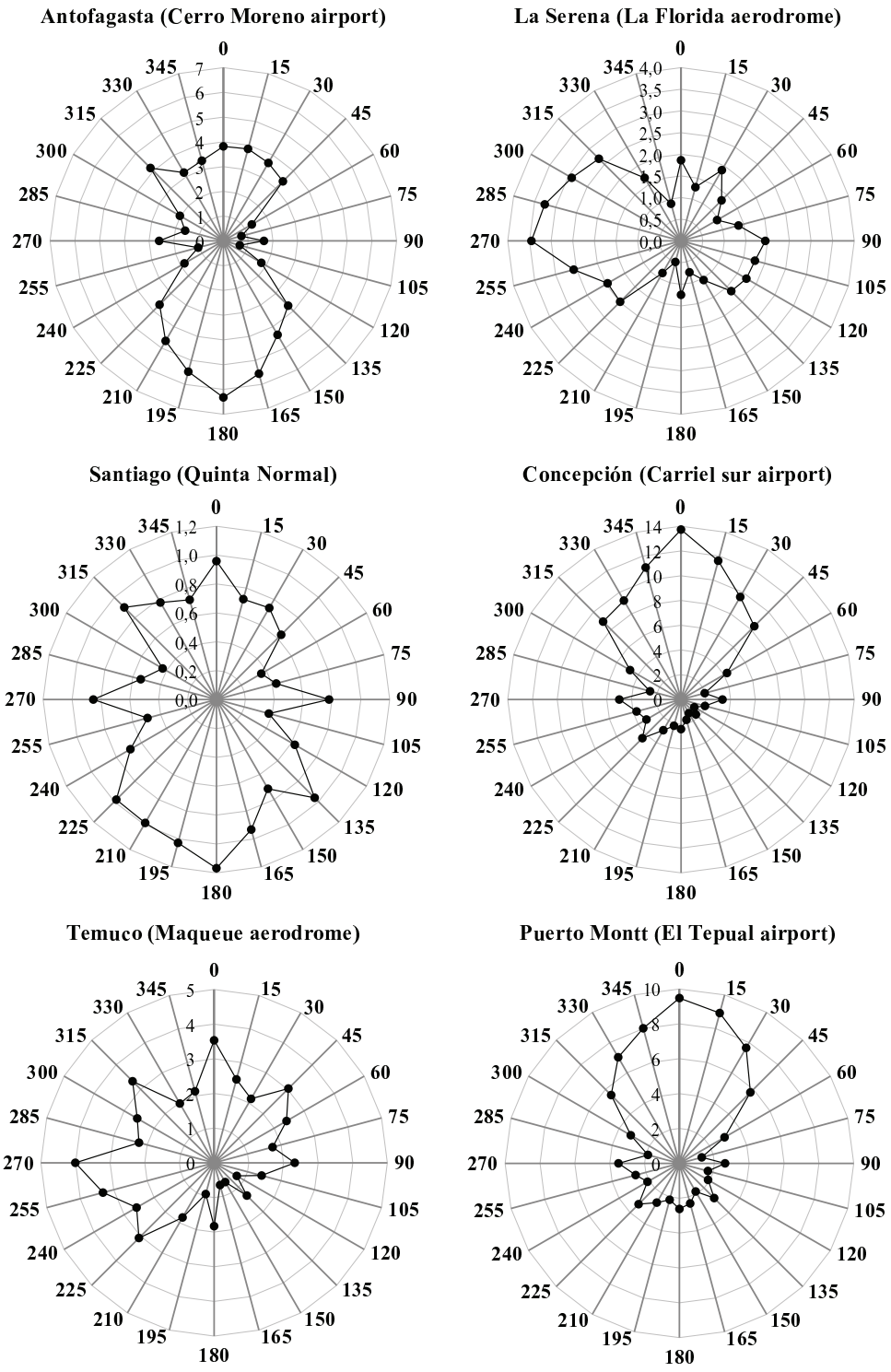

Fig. 12. Directional $DRWP_A$ values (Pa) for 6 major cities in Chile (a*ngles are measured in degrees from north*).

Figure 13

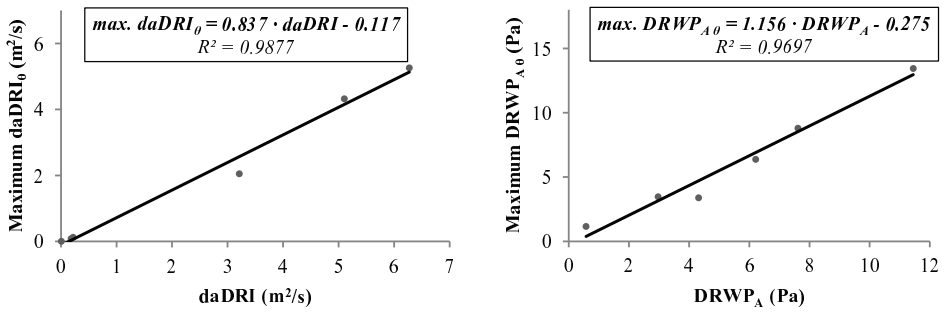

Fig. 13. Best fit-linear relationships between the scalar and maximum directional values for the WDR and DRWP exposures.